ISSN 1063-7737, Astronomy Letters, 2014, Vol. 40, No. 4, pp. 161–170. © Pleiades Publishing, Inc., 2014.
Original Russian Text © A.V. Ipatov, M.A. Kharinov, V.V. Mardyshkin, A.G. Mikhailov, Yu.N. Gnedin, M.Yu. Piotrovich, A.A. Evstigneev, A.A. Dyakov, R.Yu. Sergeev, 2014, published in Pis'ma v Astronomicheskiĭ Zhurnal, 2014, Vol. 40, No. 4, pp. 187–197.

Investigation of the Radio Emission from Active Galactic Nuclei: Determining the Spin of a Supermassive Black Hole

A. V. Ipatov[1], M. A. Kharinov[1], V. V. Mardyshkin[1], A. G. Mikhailov[1], Yu. N. Gnedin[2*], M. Yu. Piotrovich[2], A. A. Evstigneev[1], A. A. Dyakov[1], and R. Yu. Sergeev[1]

[1] *Institute of Applied Astronomy, Russian Academy of Sciences, nab. Kutuzova 10, St. Petersburg, 191187 Russia*

[2] *Pulkovo Observatory, Russian Academy of Sciences, Pulkovskoe sh. 65, St. Petersburg, 196140 Russia*

Received June 14, 2013; in final form, October 31, 2013

Abstract—The results of radio observations for ten kinetically dominated quasars are presented. The observations have been performed at 3.5 cm with the RTF-32 radio telescopes at the Zelenchukskaya and Badary observatories of the Institute of Applied Astronomy of the Russian Academy of Sciences. The kinetic power of the relativistic jets and the spins of the supermassive black holes in these objects have been determined from radio luminosity measurements. The rotation of the black hole in these objects is shown to be retrograde with respect to the Keplerian rotation in the accretion disk in the case of an approximate equality between the magnetic and gas pressures near the black hole event horizon.

DOI: 10.1134/S1063773714040021

Keywords: *radio astronomy, radio brightness distribution, active galactic nuclei, accretion, relativistic jet.*

INTRODUCTION

Valuable information about the relativistic jet production mechanism and the mechanism of interaction between the accretion disk and the outflow of matter from the accretion disk can be obtained by investigating the variability of the radio emission from active galactic nuclei (AGNs).

There are supermassive black holes in the central regions of AGNs. Two physical parameters are most important for describing such black holes (BHs): the BH mass $M_{\rm BH}$ and spin $\vec{J}_{\rm BH}$ (Dotti et al. 2013). The dimensionless spin equal to $a = J/M_{\rm BH}^2$ in the universally accepted coordinate system with $G = c = 1$ is commonly used.

In this paper, we show how the magnitude and direction of the spin of a supermassive black hole (SMBH) can be determined from the radio flux densities of several AGNs.

There are data on the spins of several AGNs in the literature (Brenneman and Reynolds 2006, 2009; de la Calle Pérez et al. 2010; Patrick et al. 2011; Brenneman et al. 2011; Reynolds 2013). In these papers, the spin was determined by analyzing the shape of spectral lines in the X-ray band of the electromagnetic spectrum. Measuring the BH spin is a critical moment for determining the cosmic evolution of massive BHs. The spin determines the efficiency of physical conversion of accreting-gas gravitational energy into accretion disk radiation. The generation of powerful relativistic jets itself depends strongly on the BH spin (Blandford and Znajek 1977). The generation of a relativistic jet results from the magnetic extraction of the rotational energy of the BH itself. In this case, the magnetic field generated near the BH event horizon plays a significant role. The radius of this horizon is defined as

$$R_{\rm H} = R_{\rm g}(1 + \sqrt{1 - a^2}), \quad R_{\rm g} = \frac{GM_{\rm BH}}{c^2}, \qquad (1)$$

where $R_{\rm H}$ is the radius of the event horizon and $R_{\rm g}$ is the gravitational radius of the BH.

The problem of determining the SMBH spin in AGNs is the focus of attention of modern astrophysics. Detailed X-ray spectra taken at the Suzaku and XMM-Newton X-ray space observatories are used to solve this problem. As a result, stringent constraints on the BH spins in a number of AGNs were obtained in the papers cited above. Nevertheless, there exists a rather large scatter of SMBH spin estimates and, therefore, any independent method that gives an estimate of the SMBH spin is useful. The spin can be determined by a standard method from the kinetic power of the relativistic jet and the magnetic field generated during accretion near the SMBH event horizon.

*E-mail: gnedin@gao.spb.ru

According to Daly (2011), the spin can be determined from the formula

$$|a| = \eta \left(\frac{L_{\rm j}}{10^{44}\ {\rm erg\ s^{-1}}}\right)^{1/2} \left(\frac{10^4\ {\rm G}}{B_{\rm H}}\right) \left(\frac{10^8 M_\odot}{M_{\rm BH}}\right), \quad (2)$$

where $L_{\rm j}$ is the kinetic power of the relativistic jet and $B_{\rm H}$ is the magnetic field generated near the BH event horizon. The coefficient η depends on the relativistic jet generation mechanism: $\eta = \sqrt{5}$ if the jet is generated during the rotation of a BH with a magnetic field on its event horizon (Blandford and Znajek 1977) and $\eta = (1.05)^{-1/2}$ if the accretion disk is also involved in the jet generation (Meier 1999). Thus, the main problem is to determine the kinetic power of the jet generated by the SMBH in an AGN and the magnetic field strength near the BH event horizon.

An expression for determining the kinetic power of a relativistic jet is presented in Merloni and Heinz (2007):

$$\log L_{\rm j} = (0.81 \pm 0.11) \log L_{\rm R} + 11.9^{+4.1}_{-4.4}, \quad (3)$$

where $L_{\rm R} = L(5\ {\rm GHz})$ is the radio luminosity of the AGN at $\nu = 5$ GHz. As regards the magnetic field strength near the BH event horizon, it is generally determined from the relation between the magnetic and accreting-gas pressures near the event horizon (Li 2002; Wang et al. 2003):

$$B_{\rm H} = \frac{\sqrt{2k\dot{M}c}}{R_{\rm H}} = 6.3 \times 10^4 \left(\frac{l_{\rm E}}{M_8}\right)^{1/2} \times \left(\frac{k}{\varepsilon}\right)^{1/2} \frac{1}{1+\sqrt{1-a^2}}\ {\rm G}, \quad (4)$$

where $M_8 = M_{\rm BH}/10^8 M_\odot$, $l_{\rm E} = L_{\rm bol}/L_{\rm Edd}$, $L_{\rm bol}$ is the bolometric luminosity of the AGN, $L_{\rm Edd} = 1.3 \times 10^{38}(M_{\rm BH}/M_\odot)$ is the Eddington luminosity, $\varepsilon(a)$ is the conversion efficiency of accreting-gas gravitational energy into radiation, i.e., $L_{\rm bol} = \varepsilon \dot{M} c^2$, where $\dot{M}$ is the accretion rate. The coefficient $k = \frac{1}{\beta} = \frac{P_{\rm mag}}{P_{\rm acc}}$ specifies the ratio of the magnetic pressure to the accreting-gas pressure on the BH event horizon $R_{\rm H}$, β is the well-known plasma parameter.

Thus, Eqs. (2)–(4) allow the BH spin to be estimated if the radio luminosity $L_{\rm R}$ of a specific AGN is known.

OBSERVATIONS AND DATA REDUCTION

In 2010–2012, ten kinetically dominated ($L_{\rm j} \gg L_{\rm bol}$) quasars (Veron-Cetty and Veron 2010) were observed. Their list is presented in Table 1, which gives: (1) the object name; (2) right ascension α; (3) declination δ; (4) redshift z (Punsly 2007), for 3C 190 (Nilsson et al. 1993); (5) the largest angular size $R_{\rm max}$, including the scatter of jets (Nilsson et al. 1993); (6) the mean flux density $S_{\rm tot}$ obtained in this paper over the period of observations 2010–2012; (7) the variability index V; (8) the normalized χ^2 value for real observations; (9) the normalized theoretical $\chi^2(0.1\%)$ value for the 0.1% significance level; (10) the number of degrees of freedom n; and (11) the number of sets of hourly observations N.

All our observations aimed at investigating AGNs were carried out at 3.5 cm (8.5 GHz) with the RTF-32 radio telescopes at the Zelenchukskaya and Badary observatories of the Institute of Applied Astronomy of the Russian Academy of Sciences (IAA RAS). All of the program sources were observed with both radio telescopes. The RTF-32 radio telescope is a quasi-parabolic mirror 32 m in diameter with a secondary quasi-hyperboloid 4 m in diameter with a focal distance of 11.4 m that has an altitude-azimuthal mounting and an rms surface error of 0.5 mm (Finkelstein 2001).

The characteristics of the RTF-32 receivers are presented in Table 2: (1) the observatory name; (2) the receiver noise temperature; (3) the antenna noise temperature (including the antenna–feeder device and the "sky"); (4) the system noise temperature; (5) the antenna effective-area coefficient; (6) the system equivalent flux density (SEFD); (7) the input frequency band width; (8) the sensitivity in flux density for the output frequency band $\Delta F = 1$ MHz according to the formula

$$P_{\rm min} = \sqrt{2} SEFD \sqrt{\frac{\Delta F}{\Delta f}}. \quad (5)$$

The observations were carried out in the regime of scanning in elevation (Ivanov et al. 2005). The program sources were observed at elevations from 40° to 70°. When determining the flux density of a program source, we took into account the change in the antenna's effective area from our observations of the reference sources 3C 295, 3C 48, 3C 309.1, 3C 286, and 3C 147. The flux densities of the reference sources were taken from Ott et al. (1994). We planned and drew up the programs of observations using the Sched Maker software (Kharinov 2006). The reference and program sources were observed in turn: the reference source during a 10–15 min set and then the program source during a one-hour set. The daily sessions were conducted, on average, once in a weak.

We reduced our observations with the Class Visual software package (Kharinov and Yablokova 2012) using the Database of Radiometric Observations (Ivanov et al. 2005). During the primary

Table 1. Parameters of the program objects

Object	$\alpha(2000)$	$\delta(2000)$	z	$R_{\max}$	$S_{\rm tot}$, mJy	V	χ^2	χ^2, 0.1%	n	N
1	2	3	4	5	6	7	8	9	10	11
3C 9	$00^{\rm h}20^{\rm m}25\overset{\rm s}{.}22$	$15°40'54\overset{''}{.}70$	2.018	$13''$	245 ± 12	0.04	0.60	1.80	43	45
3C 14	$00^{\rm h}36^{\rm m}06\overset{\rm s}{.}45$	$18°37'59\overset{''}{.}00$	1.468	$24''$	286 ± 19	0.10	1.33	1.69	55	57
3C 82	$03^{\rm h}14^{\rm m}44\overset{\rm s}{.}20$	$43°14'04\overset{''}{.}00$	2.870	–	131 ± 18	0.30	$2.11^{\hat{*}}$	1.75	48	55
3C 190	$08^{\rm h}01^{\rm m}33\overset{\rm s}{.}50$	$14°14'42\overset{''}{.}00$	1.195	$4''$	418 ± 34	0.18	$1.83^{\hat{*}}$	1.80	43	44
3C 196	$08^{\rm h}13^{\rm m}36\overset{\rm s}{.}07$	$48°13'02\overset{''}{.}70$	0.871	$5''$	2353 ± 74	0.04	1.05	1.72	51	52
3C 216	$09^{\rm h}09^{\rm m}33\overset{\rm s}{.}49$	$42°53'46\overset{''}{.}48$	0.670	$5''$	1387 ± 48	0.03	0.76	1.72	52	53
3C 270.1	$12^{\rm h}20^{\rm m}33\overset{\rm s}{.}87$	$33°43'12\overset{''}{.}01$	1.519	$12''$	530 ± 38	0.12	1.74	1.75	48	49
3C 455	$22^{\rm h}55^{\rm m}03\overset{\rm s}{.}90$	$13°13'35\overset{''}{.}00$	0.543	$4''$	414 ± 15	0.03	0.74	1.72	52	53
4C 04.81	$23^{\rm h}40^{\rm m}57\overset{\rm s}{.}97$	$04°31'15\overset{''}{.}00$	2.594	$3''$	255 ± 14	0.10	0.82	1.99	30	31
4C 25.21	$07^{\rm h}33^{\rm m}08\overset{\rm s}{.}70$	$25°36'25\overset{''}{.}00$	2.686	$7''$	94 ± 21	0.25	1.52	2.39	17	51

Table 2. Parameters of the RTF-32 receivers

Observatory	$T_{\rm rec}$, K	$T_{\rm an}$, K	$T_{\rm sys}$, K	Antenna efficiency	$SEFD$, Jy	Δf, MHz	$P_{\min}$, mJy
1	2	3	4	5	6	7	8
Zelenchukskaya	15	26	41	0.57	255	900	12
Badary	20	25	45	0.50	300	900	14

reduction in the Class Visual package, the individual counts within scans were filtered according to Fisher's test. The scans that were spoiled considerably by weather or industrial noise and were definitely unusable were rejected entirely. The final scan of the set was formed as a result of accumulation. Once the calibration signals have been taken into account, the antenna temperatures of the sources were determined by fitting the final scan with a Gaussian. During the secondary reduction in the Database of Radiometric Observations, we constructed a polynomial of the dependence of the antenna efficiency on elevation based on the references sources, which was used to calculate the flux densities of the program sources.

Based on the results of our observations, we determined the mean flux density over the entire period of observations $S_{\rm tot}$ and the variability index V for each source (Table 1). The variability index was calculated from the formula (Aller et al. 2003)

$$V = \frac{(S_{\max} - \sigma_{S_{\max}}) - (S_{\min} + \sigma_{S_{\min}})}{(S_{\max} - \sigma_{S_{\max}}) + (S_{\min} + \sigma_{S_{\min}})}, \qquad (6)$$

where $S_{\max}$ and $S_{\min}$ are the maximum and minimum flux densities over the entire period of observations.

An additional estimate of the variability for the program radio sources was made using the χ^2 test, just as in Gorshkov et al. (2011). For this purpose, we calculated the normalized χ^2 value for the total period of observations from the formula

$$\chi^2 = \frac{1}{n}\sum_i \left[\frac{S_i - S_{\rm tot}}{\Delta S_i}\right]^2, \qquad (7)$$

where $n = N_{S/\Delta S \geq 5} - 1$ is the number of degrees of freedom, S_i and ΔS_i are, respectively, the mean flux density and its error over the ith set, $S_{\rm tot}$ is the mean flux density over the entire period of observations.

When calculating all of the parameters characterizing the radio emission from our sources, we used only the measurements with a signal-to-noise ratio ≥ 5.

The variability was considered detected if the χ^2 value exceeded the value for the 0.1% significance level. Toughening the requirement for the significance

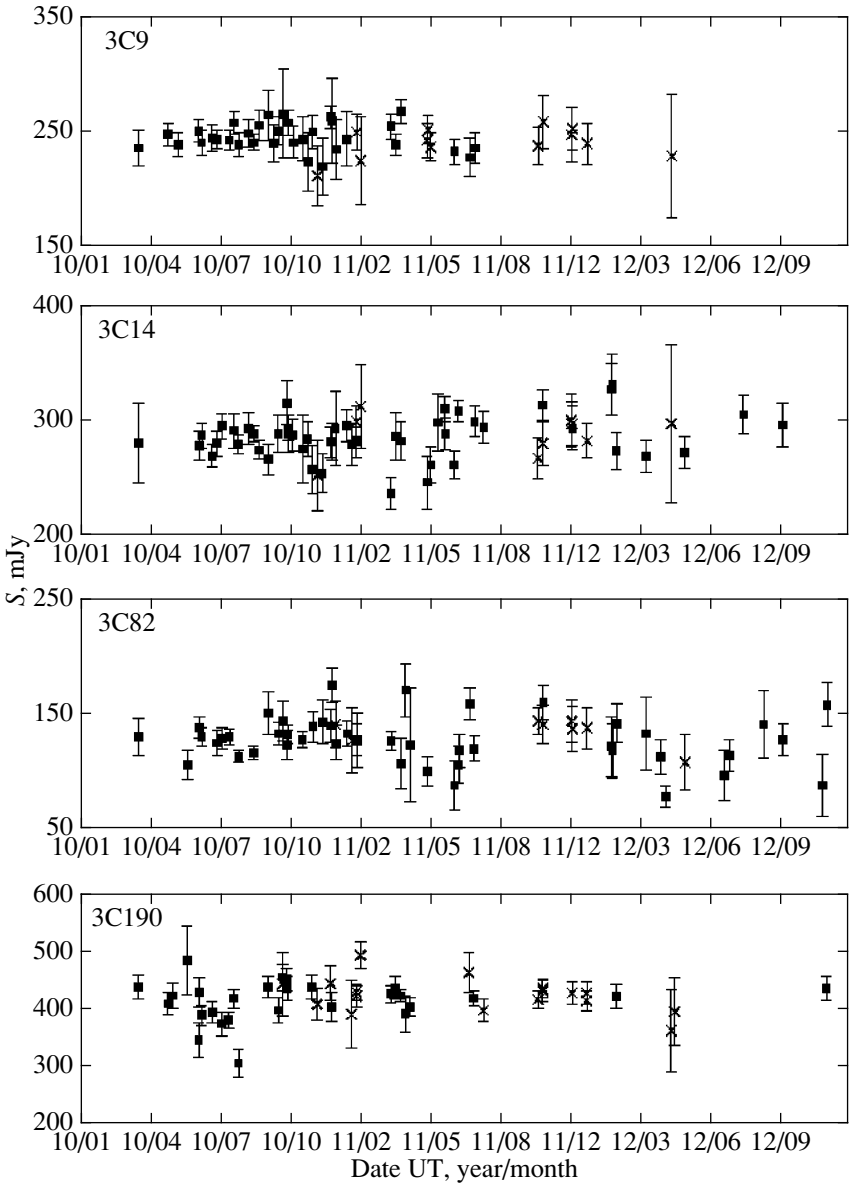

Fig. 1. Light curves of the radio sources 3C 9, 3C 14, 3C 82, and 3C 190. Each point on the plot is the flux density averaged over a one-hour set. The averagemean date (UT) of the session is along the horizontal axis and the flux density is along the vertical axis. The squares and crosses represent the observations at the Zelenchukskaya and Badary observatories, respectively.

level is related to the large number of parameters that need to be taken into account when determining the flux density in each set of observations.

The light curves of the program objects are presented in Figs. 1–3; they contain all measurements. It can be seen on the plots of the light curves that the results obtained independently at the two radio telescopes have a good correlation, which is especially noticeable in the alternation segments and the simultaneous observations at the Zelenchukskaya and Badary observatories. Consider each source separately.

3C 9 is a quasar at redshift $z = 2.018$. According to the extraneous radio observations at 2.7, 5, 10.7, and 14.9 GHz (Laing and Peacock 1980), its flux density interpolated to 8.5 GHz is $S_{\rm cat} = 271$ mJy.

Over the entire period of its observations at the IAA RAS radio telescopes, the quasar 3C 9 showed an almost constant flux density (Fig. 1) near its mean $S_{\rm tot} = 245 \pm 12$ mJy with a small variability index, $V = 0.04$. From March 25 to November 28, 2010, it was observed only at Zelenchukskaya with a constant flux density of 247 ± 10 mJy. The closest observations at the Badary and Zelenchukskaya observatories were, respectively, on December 5 and 12, 2010, with flux densities of 212 ± 26 and 220 ± 25 mJy.

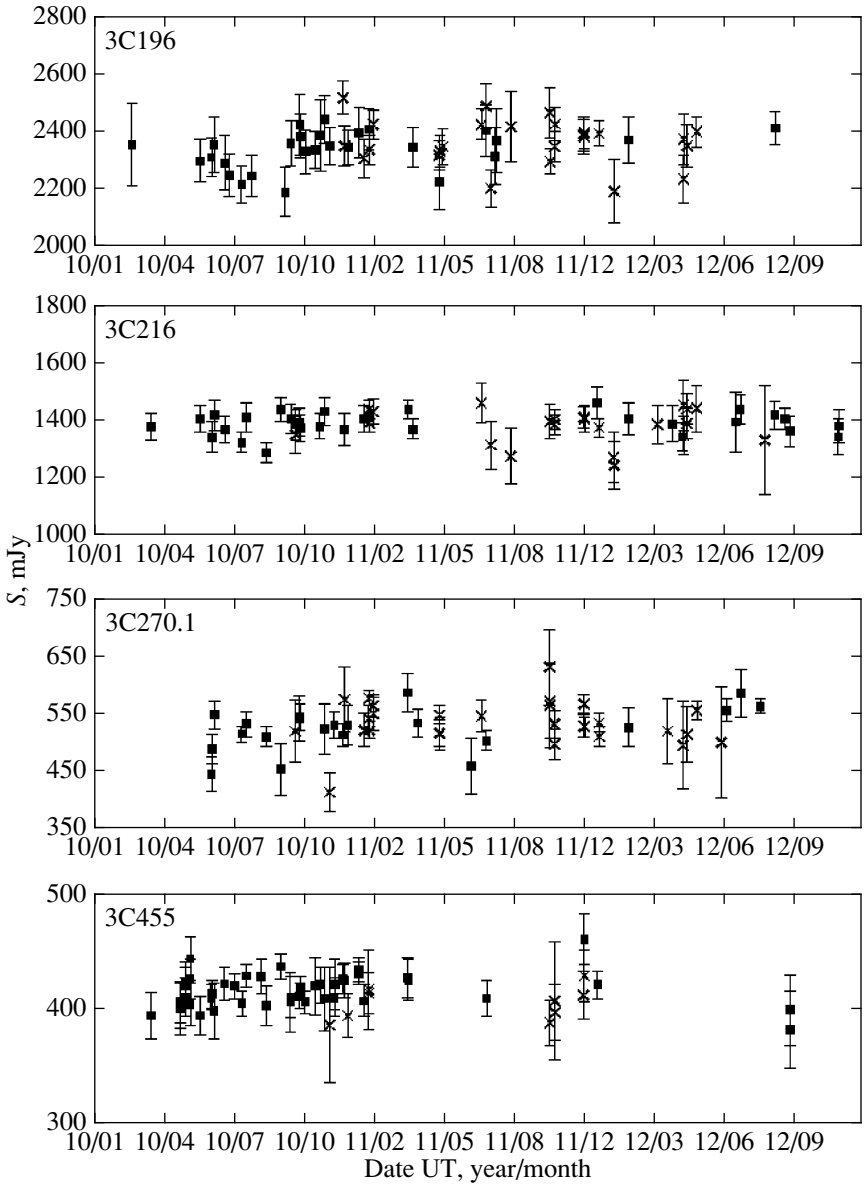

Fig. 2. Light curves of the radio sources 3C 196, 3C 216, 3C 270.1, and 3C 455. The designations are the same as those in Fig. 1.

In 2011, over two successive sessions at Zelenchukskaya, the maximum flux density $S_{\max} = 268 \pm 10$ mJy (April 3) dropped to 233 ± 10 mJy (June 19). Meanwhile, three sessions at Badary on May 11–16 showed an intermediate flux density, on average, 244 ± 8 mJy.

3C 14 is a quasar at redshift $z = 1.468$. Its interpolated flux density $S_{\text{cat}} = 292$ mJy was determined from the catalog (Laing and Peacock 1980).

The source's flux density remained constant (Fig. 1) near $S_{\text{tot}} = 286 \pm 19$ mJy with a variability index $V = 0.1$. The set-averaged minimum flux density $S_{\min} = 237 \pm 14$ mJy was recorded on March 20, 2011. Seven days later, the flux density returned to its mean level. The maximum flux density $S_{\max} = 332 \pm 27$ mJy was observed on January 29–30, 2012.

In 2011, we conducted three quasi-simultaneous sessions at Badary and Zelenchukskaya, respectively: (1) on January 30, 300 ± 13 (10 UT) and 282 ± 13 mJy (13 UT); (2) on October 23, 281 ± 20 (14 UT) and 314 ± 14 mJy (18 UT); (3) on December 4, 298 ± 19 (12 UT) and 294 ± 19 mJy (17 UT).

3C 82 is a quasar at redshift $z = 2.870$. The flux density of this source is known from other observational data only to a frequency of 5 GHz and is 282 mJy (Riley 1989).

Its variability index $V = 0.30$ was found to be the maximum one among the sources being investigated

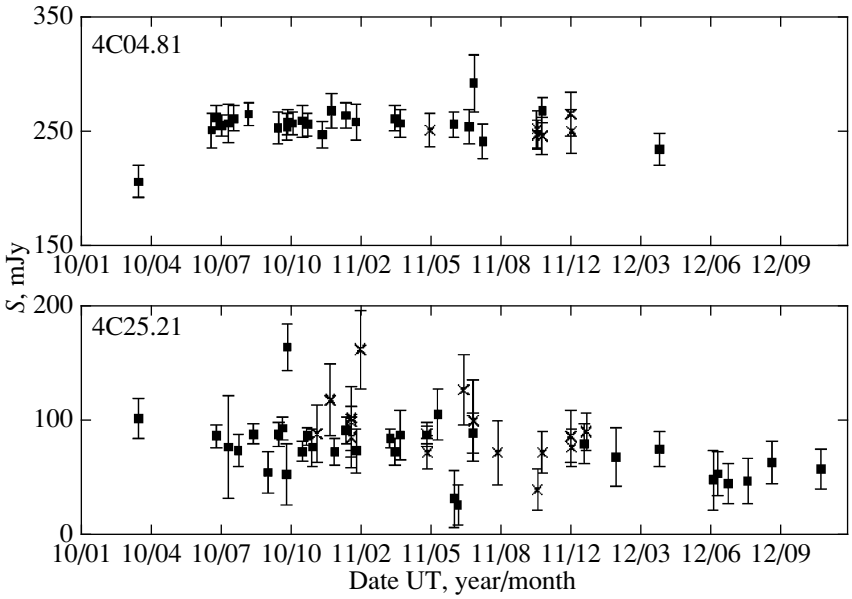

Fig. 3. Light curves of the radio sources 4C 04.81 and 4C 25.21. The designations are the same as those in Fig. 1.

here. Its long-term variability is also confirmed by the significant excess of $\chi^2 = 2.11$ above $\chi^2(0.1\%) = 1.75$. The quasar 3C 82 exhibits noticeable variability of the flux density (Fig. 1) near its mean $S_{\rm tot} = 131 \pm 18$ mJy. The maximum flux density $S_{\rm max} = 175 \pm 15$ mJy was recorded on December 26, 2010. Then, the flux density dropped until June 19, 2011, reaching 88 ± 21 mJy. The subsequent rise in flux density lasted until October 23, 2011; it reached 160 ± 15 mJy. The recurrent decay continued to the minimum flux density $S_{\rm min} = 78 \pm 9$ mJy on April 15, 2012. The period of this long-term variability of the flux density for 3C 82 can be tentatively estimated to be 11 months.

The χ^2 value exceeded the value for the 0.1% significance level.

We conducted two quasi-simultaneous sessions at Badary and Zelenchukskaya with the results coincident within one σ, respectively: (1) on December 31, 2010, 141 ± 20 (9 UT) and 125 ± 15 mJy (15 UT); (2) on October 23, 2011, 141 ± 17 (15 UT) and 160 ± 15 mJy (19 UT).

3C 190 is a quasar at redshift $z = 1.195$. The interpolated flux density of this source is $S_{\rm cat} = 479$ mJy (Laing and Peacock 1980). The appreciable variability index $V = 0.18$ is explained mainly by the initial drop in flux density (Fig. 1) to its minimum $S_{\rm min} = 306 \pm 24$ mJy on August 15, 2010. In the remaining time of its observations, the flux density remained almost constant, near its mean $S_{\rm tot} = 418 \pm 34$ mJy. There is a slight excess of $\chi^2 = 1.83$ above $\chi^2(0.1\%) = 1.80$. The weak spike, within 2σ, determined the maximum flux density $S_{\rm max} = 494 \pm 23$ mJy on February 5, 2011. The only quasi-simultaneous session was conducted at Barady and Zhelenchukskaya on October 17, 2010, with its results being 444 ± 56 (1 UT) and 456 ± 23 mJy (5 UT), respectively.

3C 196 is a quasar at redshift $z = 0.871$. The interpolated flux density of this source is $S_{\rm cat} = 2323$ mJy (Laing and Peacock 1980). No significant variability of the flux density was detected (Fig. 2). The flux density averaged over the entire period of observations was $S_{\rm tot} = 2353 \pm 74$ mJy with a variability index $V = 0.04$. The maximum flux density $S_{\rm min} = 2192 \pm 86$ mJy was recorded on October 3, 2010, after its monotonic drop that began late in June. The maximum flux density $S_{\rm max} = 2520 \pm 58$ mJy was observed on December 24, 2010.

In 2011, we conducted three quasi-simultaneous sessions at Badary and Zelenchukskaya, respectively: (1) on January 30, 2340 ± 50 (21 UT) and 2411 ± 73 mJy (17 UT); (2) on May 11, 2320 ± 51 (5 UT) and 2228 ± 99 mJy (10 UT); (3) on July 17, 2491 ± 80 (2 UT) and 2406 ± 88 mJy (5 UT).

3C 216 is a quasar at redshift $z = 0.670$. The interpolated flux density of this source is $S_{\rm cat} = 1513$ mJy (Laing and Peacock 1980). Over all 53 sessions, the flux density remained almost constant (Fig. 2) near its mean $S_{\rm tot} = 1387 \pm 48$ mJy with a variability index $V = 0.03$. The maximum flux density $S_{\rm max} = 1464 \pm 56$ mJy was recorded on December 22, 2011. One month later, on January 16, its flux density was at a minimum, $S_{\rm min} = 1245 \pm 82$ mJy.

We conducted two quasi-simultaneous sessions at Badary and Zelenchukskaya, respectively: (1) on

October 17, 2010, 1352 ± 65 (19 UT) and 1388 ± 54 (23 UT) mJy; (2) on January 30, 2011, 1441 ± 32 (14 UT) and 1416 ± 33 (2 UT) mJy.

3C 270.1 is a quasar at redshift $z = 1.519$. The interpolated flux density of this source is $S_{\rm cat} = 604$ mJy (Laing and Peacock 1980). Over the entire time of its observations, the flux density, on average, rose from 510 to 560 mJy; the flux density fluctuations along the line of the trend typically do not exceed one σ (Fig. 2). The minimum, $S_{\rm min} = 413 \pm 33$ mJy, and maximum, $S_{\rm max} = 632 \pm 66$ mJy, flux densities were observed, respectively, on December 5, 2010 and October 16, 2011. The mean flux density was $S_{\rm tot} = 530 \pm 38$ mJy with a variability index $V = 0.12$. The closest observations at Badary and Zelenchukskaya were, respectively, on December 26 and 24, 2010, with flux densities of 575 ± 56 and 513 ± 19 mJy.

3C 455 is a quasar at redshift $z = 0.543$. The interpolated flux density of this source is $S_{\rm cat} = 416$ mJy (Laing and Peacock 1980). Its flux density remained almost constant (Fig. 2) near its mean 414 ± 15 mJy with a variability index $V = 0.03$. The maximum, $S_{\rm max} = 461 \pm 22$ mJy, and minimum, $S_{\rm min} = 382 \pm 34$ mJy, flux densities were observed, respectively, on December 4, 2011 and September 23, 2012. The only quasi-simultaneous session at Badary and Zelenchukskaya was conducted on December 4, 2011, with the results, being 429 ± 23 (9 UT) and 461 ± 22 (18 UT) mJy, respectively. Since its flux density was constant, the observations of 3C 455 were reduced considerably in 2011–2012 in favor of more variable sources.

4C 04.81 is a quasar at redshift $z = 2.594$. In other observations, the flux density of this source was measured only to a frequency of 5 GHz and is 450 mJy, in accordance with the Parkes catalog (Wright and Otrupcek 1990). The flux density showed a high stability in the period from July 8, 2010 to December 4, 2011 (Fig. 3). The mean flux density over this period was 257 ± 10 mJy; the error corresponds to any result over the entire period. The reduced flux densities obtained at the very beginning and at the end of the total period of observations are of interest: $S_{\rm min} = 206 \pm 14$ mJy on March 25, 2010 and 234 ± 14 mJy on April 8, 2012. The maximum flux density $S_{\rm max} = 292 \pm 25$ mJy was recorded on July 18, 2011. As a result, the mean flux density over the entire period of observations is $S_{\rm tot} = 255 \pm 14$ mJy with a variability index $V = 0.10$. The only quasi-simultaneous session at Badary and Zhelenchukskaya was conducted on October 23, 2011, with the results being 246 ± 16 (16 UT) and 268 ± 11 (20 UT) mJy, respectively.

4C 25.21 is a quasar at redshift $z = 2.686$. The flux density of this source is known to a frequency of 5 GHz and is 200 mJy according to the Parkes catalog (Wright and Otrupcek 1990). In the entire time of its observations, the flux density decreased, on average, from 100 to 60 mJy (Fig. 3). The flux density fluctuations along the line of the trend do not exceed one σ, with the exception of several flares responsible for the variability index $V = 0.25$. The maximum flux density $S_{\rm max} = 172 \pm 21$ mJy was recorded during the October 24, 2010 flare. A similar flare with a flux density of 170 ± 36 mJy was observed on February 5, 2011, but with a lower accuracy. The minimum flux density $S_{\rm min} = 76 \pm 15$ mJy was recorded on May 12, 2011.

In 2011, we conducted two quasi-simultaneous sessions at Badary and Zelenchukskaya, respectively: (1) on May 11, 93 ± 11 (6 UT) and 92 ± 8 (11 UT) mJy; (2) on July 17, 105 ± 37 (5 UT) and 94 ± 18 (6 UT) mJy.

DETERMINING THE SMBH SPIN FROM AGN RADIO OBSERVATIONS

Based on Eqs. (2)–(4), we can estimate the BH spin:

$$f(a) = \frac{\eta}{\sqrt{k}} \times 1.81 \times \left(\frac{L_{\rm j}}{L_{\rm bol}}\right)^{1/2} = \frac{|a|}{\sqrt{\varepsilon(a)}(1+\sqrt{1-a^2})}. \quad (8)$$

Recall that $\eta = \sqrt{5}$ for the Blandford–Znajek mechanism and $\eta = 1.05^{-1/2}$ for the hybrid mechanism (i.e., the tandem of BH rotation and accreting-disk contribution (Meier 1999)). If the magnetic and accreting-plasma pressures are assumed to be equal, then the coefficient $k = 1$. The function $f(a)$ itself is presented in Fig. 4.

The scheme of our calculations will be demonstrated for the first two radio quasars from Table 3 as an example, 3C 9 and 3C 14. The cosmological redshift of 3C 9 is $z = 2.009$. This means that the emission frequency in the rest frame is $\nu_0 = 8.45(1 + z) = 25.4$ GHz. Determining the spectral distribution of emission in the rest frame of the quasar 3C 9 is the key point.

Recall that the observed radiation flux is related to the radiation power in the rest frame of a source as

$$F(\nu) = \frac{L((1+z)\nu)}{4\pi D_{\rm L}^2}(1+z), \quad (9)$$

where L is the monochromatic radiation power in the source's rest frame, $F(\nu)$ is the observed monochromatic radiation flux, and $D_{\rm L}$ is the cosmological distance to the specified source. The cosmological distance is determined as

$$D_{\rm L} = \frac{c}{H_0}(1+z)y(z), \quad y(z) = \int_0^z \frac{dx}{H(x)/H_0}. \quad (10)$$

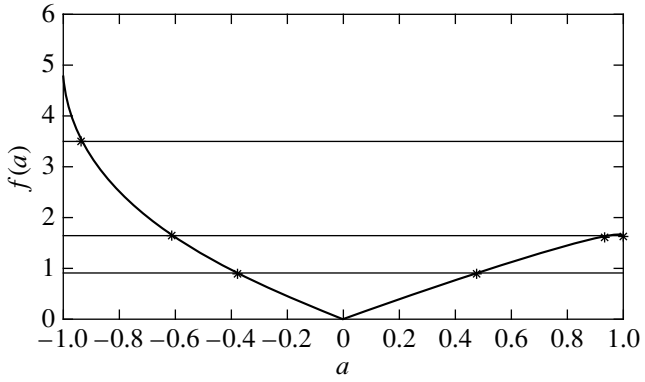

Fig. 4. Plot of the function $f(a)$.

The cosmological Hubble parameter $H(z)$ depends on cosmological redshift z as

$$H(z) = H_0[\Omega_{\rm M}(1+z)^3 + \Omega_\Lambda], \qquad (11)$$

where $\Omega_{\rm M} = 0.27$ is a dimensionless parameter characterizing the mean density of the Universe with dark matter, Ω_Λ is a dimensionless parameter specifying the contribution of dark energy: $\Omega_\Lambda = 0.73$.

Calculating the monochromatic luminosity at $\nu = 5$ GHz in the rest frame of an object is the key point. It is the luminosity $\nu L(\nu)$ at $\nu = 5$ GHz that accounts for a significant fraction of the AGN radio luminosity $L_{\rm R}$.

According to Merloni and Heinz (2007), the radio luminosity $L_{\rm R}$ allows the kinetic power of the relativistic jet to be estimated:

$$L_{\rm j} = 10^{11.9}(L_{\rm R})^{0.81}. \qquad (12)$$

Table 3. Spin determinations for the observed objects

Object	Hybrid model		Blandford–Znajek mechanism	
	a	k	a	k
3C 9	−0.998	1.0	−0.998	2.0
3C 14	−0.85	1.0	−0.998	1.2
3C 82	−0.998	1.8	−0.998	2.0
3C 190	−0.9	1.0	−0.9	2.2
3C 196	−0.9	1.0	−0.998	1.27
3C 216	−0.998	16	−0.998	7.3
3C 270.1	−0.5	1.0	−0.95	1.0
3C 455	−0.998	2.44	−0.998	11.0
4C 04.81	−0.9	1.0	−0.998	1.5
4C 25.21	−0.95	1.0	−0.998	3.03

Recall that Eq. (12) was derived by taking into account an additional effect, namely the Doppler boosting of radiation from the relativistic jet. Merloni and Heinz (2007) analyzed the distribution of mean Lorentz factors for relativistic jets and showed this distribution to have a maximum at the Lorentz factor $\Gamma_{\rm m} = 7$. It is this value that the above authors used in deriving Eq. (12).

Thus, the monochromatic radio luminosity ($\nu = 5$ GHz) should be related to the observed intensity and luminosity at $\nu = 8.5$ GHz. We will assume a power-law spectral distribution of radio emission with an index $\alpha = -0.5$. This allows the rest-frame monochromatic radio luminosity at 5 GHz to be estimated as

$$L_{\rm rest}(5\ {\rm GHz}) = L(8.5(1+z)\ {\rm GHz}) \qquad (13)$$
$$\times \left(\frac{5}{8.5(1+z)}\right)^{1/2},$$

where the luminosity $L(8.5(1+z)$ GHz) is defined by Eq. (9). Next, using Eq. (6) and Fig. 4, we obtain the SMBH spin for a given object presented in Table 3.

As the second example, consider the radio source 3C 14. This object is a quasar at cosmological redshift $z = 1.469$. In the period of observations of this object, its flux density varied periodically within the range from 270 to 332 mJy. The mean flux density was 296 ± 53 mJy. The light curve of this object over the entire period of its observations is presented in Fig. 1. As a result, according to (12) and (13), the kinetic power of the jet was estimated to be $L_{\rm j} = 10^{46.8}$ erg s^{-1}. At the same time, the bolometric luminosity of 3C 14 is $L_{\rm bol} = 3.26 \times 10^{46}$ erg s^{-1} (Punsly 2007). This allows the following expressions for determining the SMBH spin to be derived (using Eq. (8)):

$$f(a) = \frac{5.72}{\sqrt{k}}, \qquad (14)$$

Blandford–Znajek process;

$$f(a) = \frac{2.56}{\sqrt{k}}, \quad \text{Meier's hybrid model.}$$

If the magnetic and accreting-gas pressures are assumed to be equal on the BH event horizon (see (4)), then solution (14) yield $a = -0.85$ for the hybrid model. For the Blandford–Znajek process, $a = -0.998$ corresponds to the parameter $k = 1.2$, i.e., higher than unity. Thus, if the ratio of the magnetic and accreting-gas pressures on the event horizon is assumed to be no greater than 10, i.e., $k < 10$, then it can be assumed with a high probability that there is retrograde rotation of the SMBH in the case of 3C 14.

The spin determinations for other observed objects are presented in Table 3.

We emphasize that the results presented in Table 3 correspond to the case where the magnetic and accreting-gas pressures are assumed to be equal, i.e., $k = 1$, or where the ratio of these quantities corresponds to a minimum value close to unity. If we consider the case where the directions of rotation of the BH and the Keplerian disk coincide, i.e., $a > 0$, then this situation requires that the magnetic pressure be much greater than the accreting-gas pressure, i.e., $k \gg 1$. For example, the pressure ratio for the radio quasar 3C 9 takes on the following values: $a = 0.998$, $k = 3.12$ for the hybrid model and $k = 5.93$ for the Blandford–Znajek process.

The following circumstance should also be noted. When obtaining the data presented in Table 3, we used the index $n = -0.5$ in the power-law spectral distribution of radio emission. If a different value, for example, for example, $n = -1$, is used, then this will lead to the following changes. In this case, instead of Eq. (13) we obtain

$$L_{\text{rest}}(5\ \text{GHz}) = L(8.5(1+z)\ \text{GHz}). \qquad (15)$$

As a result, according to (10), the kinetic power of the relativistic jet increases. This leads to the following changes in the data of Table 3: the spins do not change significantly, but the parameter k specifying the ratio of the magnetic and radiation pressures increases. Our calculations show that the pressure ratio, i.e., the coefficient k, increases approximately by a factor of 2, exactly by a factor of 2 for the radio quasars 3C 82, 4C 25.21, 4C 04.81, and 3C 27.01. For 3C 9, the new value of k turns out to be a factor of 1.9 larger than the value given in Table 3.

CONCLUSIONS

We performed long-term (2010–2012) radio observations of ten kinetically dominated quasars with the RTF-32 radio telescopes at the Zelenchukskaya and Badary observatories of the IAA RAS. All of the observed objects are characterized by a high radio luminosity; they may be considered as kinetically powerful, i.e., according to Punsly (2007), kinetically dominated objects.

Long-term variability of the flux density, within 88–175 and 306–494 mJy, respectively, was detected for the radio sources 3C 82 and 3C 190. For the remaining objects, the flux density remained constant within 2σ, in agreement with the well-known reviews (Laing and Peacock 1980; Riley 1989).

Based on our radio luminosity measurements, we determined the kinetic power of the relativistic jet in the rest frame of a specific AGN. The estimated kinetic powers of the jets in these objects allowed the spins of the rotating SMBHs hosted by the observed AGNs to be determined. We used the expression for the magnetic field strength in which the magnetic and gas pressures were assumed to be equal on the event horizon of the accreting central BH. The main result is that, when the pressures are equal, the SMBHs in these objects are in retrograde rotation with respect to the accretion disk. Prograde rotation can be realized only in the case where the magnetic pressure near the event horizon is considerably higher than the accreting-gas pressure.

ACKNOWLEDGMENTS

This work was supported by Program no. 21 of the Presidium of the Russian Academy of Sciences and Program no. 17 of the Division of Physical Sciences of the Russian Academy of Sciences. M.Yu. Piotrovich thanks the Russian Foundation for Basic Research (project no. 12-02-31500-mol_a) for support.

REFERENCES

1. M. F. Aller, H. D. Aller, and P. A. Hughes, Astrophys. J. **586**, 33 (2003).
2. R. D. Blandford and R. L. Znajek, Mon. Not. R. Astron. Soc. **216**, 65 (1977).
3. L. W. Brenneman, C. S. Reynolds, M. A. Nowak, et al., Astrophys. J. **736**, 103 (2011).
4. L. W. Brenneman and C. S. Reynolds, Astrophys. J. **652**, 1028 (2006).
5. L. W. Brenneman and C. S. Reynolds, Astrophys. J. **702**, 1367 (2009).
6. I. de la Calle Pérez, A. L. Longinoti, M. Guainazzi, et al., Astron. Astrophys. **524**, 50 (2010).
7. R. Daly, Mon. Not. R. Astron. Soc. **414**, 1253 (2011).
8. M. Dotti, M. Colpi, S. Pallini, et al., Astrophys. J. **762**, 68 (2013).
9. A. M. Finkelshtein, Nauka Rossii **5**, 20 (2001).
10. A. G. Gorshkov, A. V. Ipatov, V. K. Konnikova, et al., Astron. Rep. **55**, 1096 (2011).
11. D. V. Ivanov, A. V. Ipatov, I. A. Ipatova, et al., Tr. IPA RAN **12**, 93 (2005).
12. M. A. Kharinov, Tr. IPA RAN **13**, 15 (2006).

13. M. A. Kharinov and A. E. Yablokova, Tr. IPA RAN **24**, 342 (2012).
14. R. A. Laing and J. A. Peacock, Mon. Not. R. Astron. Soc. **190**, 903 (1980).
15. L. X. Li, Astron. Astrophys. **392**, 469 (2002).
16. D. L. Meier, Astrophys. J. **522**, 753 (1999).
17. A. Merloni and S. Heinz, Mon. Not. R. Astron. Soc. **381**, 589 (2007).
18. K. Nilsson, M. J. Valtonen, J. Kotilainen, and N. Jaakkola, Astrophys. J. **413**, 453 (1993).
19. M. Ott, A. Witzel, A. Quirrenbach, et al., Astron. Astrophys. **284**, 331 (1994).
20. A. R. Patrick, J. N. Reeves, A. P. Lobban, et al., Mon. Not. R. Astron. Soc. **416**, 2725 (2011).
21. B. Punsly, Mon. Not. R. Astron. Soc. **374**, L10 (2007).
22. C. S. Reynolds, arXiv:1307.3246 (2013).
23. J. M. Riley, Mon. Not. R. Astron. Soc. **238**, 1055 (1989).
24. M. P. Veron-Cetty and P. Veron, Astron. Astrophys. **518**, A10 (2010).
25. D.-X. Wang, R.-Y. Ma, W.-H. Lei, and B.-Z. Yao, Astrophys. J. **595**, 109 (2003).
26. A. Wright and R. Otrupcek, *Parkes Catalog* (Australia Telescope National Facility, 1990).

Translated by V. Astakhov